Electromagnetically induced transparency: the thickness of the vapor column is of the order of a light wavelength

Y. Pashayan-Leroy,[1] C. Leroy,[1] A. Sargsyan,[2] A. Papoyan,[2] and D. Sarkisyan[2,*]

[1]*Institut Carnot de Bourgogne, UMR 5209 CNRS-Universit de Bourgogne, 9 Av. A Savary, BP47 870, F–21078 Dijon Cedex, France*

[2]*Institute for Physical Research, National Academy of Sciences of Armenia, Ashtarak, 0203 Armenia*

**Corresponding author: david@ipr.sc.am*

Received November 28, 2006; revised March 12, 2007; accepted April 19, 2007; posted April 30, 2007 (Doc. ID 77263); published July 19, 2007

Electromagnetically induced transparency (EIT) effect has been studied using an extremely thin cell (ETC) with the thickness of an Rb vapor column of the order of light wavelength λ (780 nm) and varying in the range of 0.5λ–2.5λ. Λ-systems on the D_2 line of ^{85}Rb and ^{87}Rb have been studied experimentally. Along with EIT resonance, we study the peculiarities of velocity-selective optical pumping/saturation (VSOP) resonances, which accompany the EIT resonance and, as a rule, are spectrally broader. It is demonstrated that size-conditioned strongly anisotropic contribution of atoms with different velocities in an ETC causes several dramatic differences of the EIT and VSOP resonances formation in the ETC as compared with an ordinary 1–10 cm long cell. Particularly, in the case of the ETC, the EIT linewidth and contrast dramatically depend on the coupling laser detuning from the exact atomic transition. A theoretical model taking into account the peculiarities of transmission spectra when $L=n\lambda$ and $L=(2n+1)\lambda/2$ (n is an integer) has been developed. The experimental transmission spectra are well described by the theoretical model developed. The possibility of EIT resonance formation when atomic column thickness is of the order of $L=0.5\lambda$ and less is theoretically predicted.

OCIS codes: 020.1670, 020.3690, 020.2930, 300.6360.

1. INTRODUCTION

There has been considerable interest in recent years about the fascinating properties of coherent population trapping (CPT) and the related electromagnetically induced transparency (EIT). The EIT and CPT resonances can occur in a Λ-system with two long-lived states and one excited state coupled by two laser fields [1–4]. Note that alkali-metal vapor is very convenient for EIT and CPT studies, and these effects have been successfully demonstrated in atomic media prepared in a cell of ordinary length (1–100 mm). Also of considerable interest is the study of the possibility for miniaturization of alkali cells for application in the CPT (EIT) experiments without compromising the CPT resonance parameters. However, the reduction of the vapor cell size results in an increase of the dephasing rate of coherence between the ground states: $\Gamma_{21}=(2\pi t)^{-1}$, where $t=L/u$, with L being the distance between cell windows and u being the most probable thermal velocity. The latter leads to broadening of CPT and EIT resonances, as well as to worsening of the EIT resonance contrast (defined as the ratio of the EIT depth to the height of the shoulders of the EIT window). To prevent atom-window collisions for the case of submillimeter thin cells, either buffer gas or paraffin-coated walls are used [5–7]. Nevertheless, in Ref. [8], it was theoretically predicted for the cell with the thickness of $L\sim 10\ \mu$m that even in the case of pure vapor, narrow EIT resonance can be observed. Very recently it has been experimentally demonstrated that it is possible to observe EIT resonance using the so-called extremely thin cell (ETC) with an atomic vapor layer smoothly controllable in the range of $L\sim 780-1600$ nm comparable with the laser radiation wavelength resonant with the Rb D_2 line ($\lambda=780$ nm) [9]. The ETC was filled with pure Rb, neither buffer gas nor paraffin-coated walls were used. Note, that the EIT resonance linewidth in the ETC is narrower than that of the velocity-selective optical pumping or saturation (VSOP) resonance accompanying the EIT resonance. The explanation is that the contribution of atoms with a small velocity projection in the laser radiation direction (i.e., atoms flying nearly parallel to the cell windows) is enhanced thanks to their longer interaction time with laser field. Due to this atomic velocity-selectivity, the observed linewidth of the EIT resonance is more than by an order narrower than that expected from the inverse of the window-to-window flight time of the atoms. It should be noted that in accordance with its physical nature, the VSOP resonance cannot have a width narrower than the natural width of the atomic transition. As for EIT resonance, its width can be considerably narrower than the natural width [2–4]. However, the increase of the interaction time with a laser can lead to the increase of the VSOP resonance amplitude and the reduction of the EIT linewidth (see Fig. 9).

In [9] we compared our experimental results with the theoretical model of [8] as there was no other relevant model. However, this theoretical model considers a very simplified three-level system for a 10 μm thin atomic va-

por column and does not take into account the following points: (i) the influence of the reflected beam by the second wall of the ETC (which is important in the case when the thickness is $L \sim \lambda$), (ii) as shown [4] in a real atom, the ground-state coherence can be influenced by the hyperfine structure of the excited state. Thus, the hyperfine structure of $5P_{3/2}$ should be included, (iii) the influence of the Dicke-type coherent narrowing effect, which depends on the ratio L/λ should be included; (iv) the three-level model of [8] does not allow one to study the peculiarities of the supplementary VSOP resonances (which appear because of the additional upper levels); (v) such important experimental parameters, as linewidth of the coupling and probe lasers, were not included in the model; (vi) the model was applied to a 10 μm thin atomic vapor column, meanwhile for the ETC [10], the thickness of the atomic vapor is less by an order. In this work, a theoretical model including the practically all-important experimental parameters determining the EIT process as well as VSOP resonance formation in the ETC has been developed, and a comparison with the experiment is provided.

2. EXPERIMENT

The experimental setup is similar to that presented in [9]. The radiation beams ($\oslash = 3$ mm) of two single-frequency diode lasers with $\lambda = 780$ nm and the spectral width of $\gamma_L = 5$ MHz are well superposed and focused by an $F = 35$ cm lens into the ETC at nearly normal incidence. The wedge-shaped (vertical) thickness L of the gap allows one to smoothly vary the thickness of the Rb atomic vapor column in the range from 350 to 2800 nm. This ETC operates with an oven made from nonmagnetic materials and was placed inside the three pairs of mutually perpendicular Helmholtz coils providing the possibility to cancel the laboratory magnetic field as well as to apply the homogeneous magnetic field. The laboratory magnetic field was compensated with the accuracy of a few microtesla. It is easy to show that an additional broadening of the EIT resonance by the residual magnetic field is less than 0.1 MHz. The frequency reference spectra formation has been realized with an auxiliary ETC (mentioned further as ETC1) with the fixed thickness $L = \lambda$ [9]. Our Λ-type system is formed on the atomic D_2 line of ^{87}Rb (or ^{85}Rb). The ground-state hyperfine levels $F_g = 1$ and $F_g = 2$, spaced by 6835 MHz (or $F_g = 2$ and $F_g = 3$ spaced by 3036 MHz), serve as the two lower states, and the excited state $5P_{3/2}$ serves as the common upper level (see Fig. 1). The coupling laser frequency is fixed and is resonant either with the ^{87}Rb $F_g = 2 \rightarrow F_e = 2$ and $F_g = 2 \rightarrow F_e = 1$ transitions, or with the ^{85}Rb $F_g = 3 \rightarrow F_e = 3$ and $F_g = 3 \rightarrow F_e = 2$ transitions (in some cases it is blue- or redshifted from these transitions). The coupling laser frequency stabilization has been realized by using a separate ETC with the thickness $L = \lambda/2$; this technique will be published elsewhere [11]. The probe laser frequency is scanned across ^{87}Rb $F_g = 1 \rightarrow F_e = 0, 1, 2$ (^{85}Rb, $F_g = 2 \rightarrow F_e = 1, 2, 3$) transitions. The power of the coupling and probe lasers is ~ 1 mW and ~ 0.3 mW, respectively. The temperature at the window T_w and at the reservoir T_R (the reservoir temperature determines the atomic density inside the ETC) are $\sim 170\,^{\circ}$C and 150°C, respectively. These values for the reference ETC1 are 120°C and 100°C, respectively.

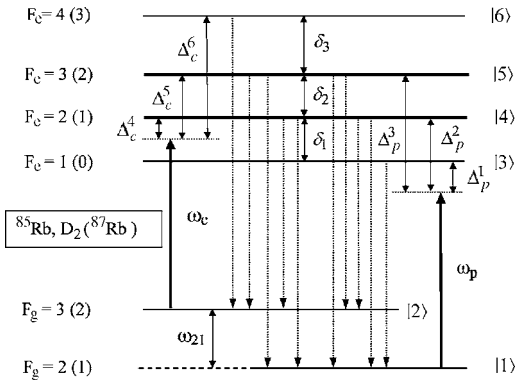

Fig. 1. Energy level diagram of the six-level model.

As demonstrated [12–15] transmission spectra of the probe laser in the case of ETC depend on the parameter L/λ. For low pump intensity (<1 mW/cm^2), the hyperfine absorption linewidth exhibits oscillating behavior, with minimum value for $L = (2n+1)\lambda/2$, and maximum value for $L = n\lambda$. This is the manifestation of so-called collapse and revival of the Dicke-type coherent narrowing effect. For high pump intensity (>1 mW/cm^2), the VSOP resonances of reduced absorption, caused by VSOP effects and centered on the hyperfine transitions occur preferentially when $L = n\lambda$, while for $L = (2n+1)\lambda/2$, the revival of peaks of increased absorption is still observable with a lower contrast. As the most interesting features are observed for $n\lambda/2$ thicknesses, $L = \lambda$, 1.5λ, 2λ, and 2.5λ values have been exploited in the experiments as well as for the numerical calculations. These thicknesses could be easily determined in the experiment by minimal reflection from the ETC's gap [12]. The ETC had the area of uniform thickness, a little less than 1 mm^2, smoothly varying in the vertical direction in the range of $\sim 0.5\lambda - 3\lambda$. That is why by slightly focusing the beam up to the diameter ~ 1 mm, we have a uniform thickness inside the beam. When using $L = \lambda, 2\lambda$ under the condition of exact resonance of the coupling laser with the corresponding atomic transition, as a rule, the transmission spectrum of the probe contains the EIT resonance, together with the VSOP resonance of reduced absorption peak, which are superimposed on the frequency scale and contribute in the same way leading to absorption reduction. Meanwhile when using $L = 1.5\lambda, 2.5\lambda$ under the condition of exact resonance, the transmission spectrum of the probe contains the EIT resonance, together with the revival peaks of the increased absorption, which are superimposed on the frequency scale and contribute with opposite sign. These features are well seen on the experimental as well as on the calculated curves.

3. OUTLINE OF THE MODEL

Modeling of EIT is achieved by considering three-level atomic systems. In fact, most real atomic manifolds are made up of a multiple of levels. For example, in the case of D_2 transition of Rb, there is a set of four closely spaced upper levels. To interpret our experimental results, we consider the six-level hyperfine structure of Rb D_2 transition as shown in Fig. 1. The energy levels are denoted as

$i=1,2,3,4,5,6$ and δ_1, δ_2, δ_3 are the hyperfine splittings of the upper state. A vapor of the six-level atoms confined in an ETC of thickness L is excited under normal incidence by two copropagating electromagnetic fields. Level $|2\rangle$ is coupled to levels $|4\rangle$, $|5\rangle$, and $|6\rangle$ by the intense laser $E_c(z,t)$ with frequency ω_c (the coupling field). The weak laser $E_p(z,t)$ with frequency ω_p(the probe field) couples level $|1\rangle$ to levels $|3\rangle$, $|4\rangle$, and $|5\rangle$. In a Doppler-broadened system, the frequency detunings from the resonance of the probe and coupling fields are defined as

$$\Delta_p^{1,2,3} = \omega_{i1} - \omega_p \pm k_p v_z \quad (i=3,4,5), \tag{1}$$

$$\Delta_c^{4,5,6} = \omega_{i2} - \omega_c \pm k_c v_z \quad (i=4,5,6), \tag{2}$$

where $\omega_{i,k}$ is the energy difference between the levels i and k. Here $k_{p,c}v_z$ is the Doppler shift contribution for the detuning of the laser field corresponding to the velocity component v_z along the propagation vector $\mathbf{k}_{p,c}$. The plus sign refers to the atoms with the velocity $\mathbf{v}$ in the positive direction of the cell axis, and the minus sign refers to the atoms with the velocity $\mathbf{v}$ in the negative direction of the cell axis.

Our theoretical calculations are based on a standard density-matrix approach. The dynamical behavior of the density matrix ρ is given by the Liouville equation of motion:

$$\frac{d\rho}{dt} = -\frac{i}{\hbar}[H,\rho] + \Lambda\rho. \tag{3}$$

Here H is the Hamiltonian of the six-level atom including the dipole interaction with the bichromatic laser radiation, and Λ is the relaxation matrix. All spontaneous emission rates of the excited states are assumed to be the same, and all ground level population relaxation rates are ignored under the assumption that the ground states are stable. We assume that the atomic density N is low enough so that only atom-surface collisions are to be considered. Consistent with this condition, we ignore collisional broadening γ^{col} in our theoretical model, but we consider a relaxation rate Γ_{21} for the coherence between the ground-state levels, which is dominated by the finite time of flight of atoms between the cell windows. We also assume that the atoms lose optical excitation and all memory about the previous state when colliding with the cell windows, and that the incident laser beam diameter largely exceeds the cell thickness. With the assumptions made, the relaxation effect is taken into account exactly by solving the temporal density-matrix equations with proper boundary conditions for each atom separately. We neglect the magnetic substructure of each level.

The relaxation Γ_{21} is also sensitive to amplitude or phase fluctuations of the laser fields. We use the Wiener–Levy phase diffusion model (see, e.g., [16–18]) to describe the effects of the finite bandwidth of the laser field to the coherence of the interaction. We assume that both lasers have a Lorentzian spectrum with a full frequency width at half maximum (FWHM) γ_L (as obtained from the model adopted). The laser bandwidths are incorporated into the calculations by introducing relaxation terms for the nondiagonal density-matrix elements using the procedure developed in [19,20].

Polarization of the medium on the frequency of the probe field is determined by

$$P(z) = N\sum_{j=3}^{5} \mu_{j1}(\rho_{j1}^{+} + \rho_{j1}^{-}), \tag{4}$$

where nondiagonal matrix elements $\rho_{j1}^{+} \equiv \rho_{j1}\,(z=v_z t)$ and $\rho_{j1}^{-} \equiv \rho_{j1}\,(z=L-v_z t)$ relate to the atoms flying with the velocity in the positive and negatives directions of the cell axis, respectively. Here μ_{j1} $(j=3,4,5)$ is the electric dipole moment of the optical transition $|j\rangle \rightarrow |1\rangle$.

We obtain absorption spectra by calculating numerically the set of density-matrix equations (see Appendix A for the complete equations of motion). Details for the theoretical modeling appear in [13,21]. The absorption of the probe beam is determined by the sum of imaginary parts of three atomic coherences, i.e., Im ρ_{31}, Im ρ_{41}, and Im ρ_{51}. The differential equations of these coherences read

$$\dot{\rho}_{31} = i\Omega_1(\rho_{11}-\rho_{33}) - i\Omega_2\rho_{34} - i\Omega_3\rho_{35} - [i\Delta_p^1 + \Gamma_{31}]\rho_{31}, \tag{5}$$

$$\dot{\rho}_{41} = i\Omega_2(\rho_{11}-\rho_{44}) + i\Omega_4\rho_{21} - i\Omega_1\rho_{43} - i\Omega_3\rho_{45} - [i\Delta_p^2 + \Gamma_{41}]\rho_{41}, \tag{6}$$

$$\dot{\rho}_{51} = i\Omega_3(\rho_{11}-\rho_{55}) + i\Omega_5\rho_{21} - i\Omega_1\rho_{51} - i\Omega_2\rho_{54} - [i\Delta_p^3 + \Gamma_{51}]\rho_{51}. \tag{7}$$

Ω_i $(i=1,2,3)$ and Ω_j $(j=4,5,6)$ are the Rabi frequencies of the probe and couple fields, respectively, and Γ_{ij} are the decoherence rates (for the definition see Appendix A).

To include the Doppler-broadening effect, we average the density-matrix element obtained for a single atom over the Maxwellian velocity distribution of the atoms under consideration. This is given by $W(v)=(N/u\sqrt{\pi})\exp(-v^2/u^2)$, where v is the atomic velocity, N is the atomic density, and u is the most probable velocity given by $u=\sqrt{2k_BT/M}$ with T being the temperature in Kelvin and M being the atomic mass. The Doppler broadened absorption profile is given by

$$\frac{1}{E_p^2}\langle A\rangle = -\frac{4\pi\omega_p N t_2^2 t_1}{cu\sqrt{u}}\frac{1}{E_p|F|^2}\int_0^{\infty} e^{-v_z^2/u^2} v_z dv_z \int_0^{L/v} dt \times \mathrm{Im}\left\{\sum_{i=3}^{5}\mu_{i1}[\rho_{i1}^{+}(t,\Delta^{+},E_{p0}(v_z t))(1-r_1 e^{2ik_p v_z t}) + \rho_{i1}^{-}(t,\Delta^{-},E_{p0}(L-v_z t))(1-r_1 e^{2ik_p(L-v_z t)})]\right\}. \tag{8}$$

Here t_1 and t_2 are the transmission coefficients of the cell windows; r_1 and r_2 are the reflections coefficients of the windows. All the spectra presented in Section 4 are calculated for $r_1=r_2=0.3$. The factor $F=1-r_1r_2\exp(2ikL)$ takes into account the Fabry–Perot nature of the cell caused by two highly parallel cell windows. The influence of the Fabry–Perot effect on the absorption line shape and magnitude in an ETC has been studied theoretically in [13]. The probe field inside the empty cell $E_{p0}(z)$ is defined in a way:

$$E_{p0}(z) = \frac{E_p t_1}{F}[1 - r_2 e^{2ik(L-z)}], \quad (9)$$

with E_p being an external probe field. We numerically integrate Eq. (8) and obtain a velocity-averaged absorption coefficient as a function of Raman detuning $\Delta_R = \Delta_p - \Delta_c + \omega_{21}$.

4. RESULTS AND DISCUSSIONS

In Fig. 2(a), the experimental transmission spectra of the probe laser are presented for the case where the coupling laser is resonant with the ^{87}Rb $F_g=2 \rightarrow F_e=2$ transition, while the probe laser is scanned across $F_g=1 \rightarrow F_e=0,1,2$ transitions (see the upper-left inset). This measurement was done for the ETC thickness $L=\lambda$ (780 nm). The EIT resonance is seen on the upper curve together with VSOP, and the upper inset presents the results of fitting by Lorentzian profiles. FWHM of the EIT and VSOP resonances are ~12 MHz and ~30 MHz, correspondingly

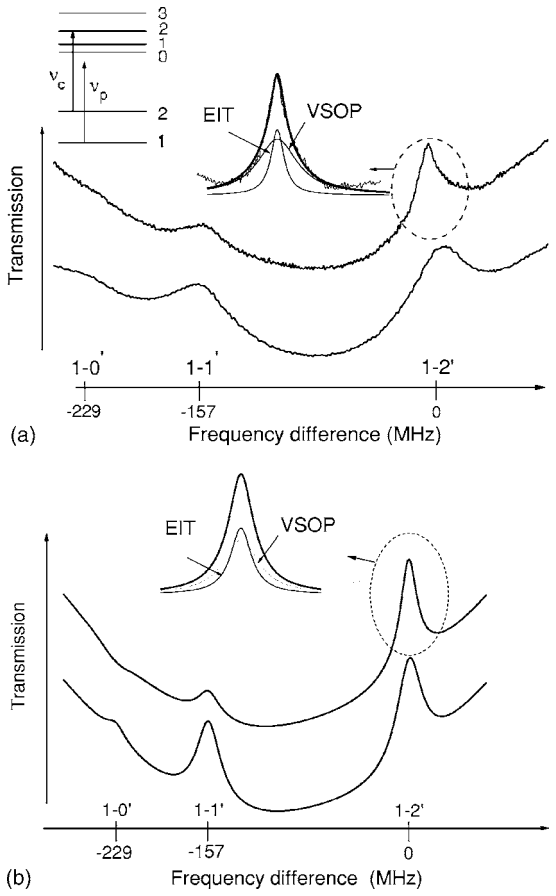

Fig. 2. Transmission spectra of the probe laser scanned across ^{87}Rb $F_g=1 \rightarrow F_e=0,1,2$ transitions (the relevant energy levels of ^{87}Rb are presented in the upper-left inset), when the coupling laser is resonant with $F_g=2 \rightarrow F_e=2$ transition. The cell thickness $L=\lambda$ (780 nm), $\gamma_L=5$ MHz. (a) Experimental results. The upper inset presents results of the fitting by Lorentzian profiles. FWHM of the EIT and VSOP resonances are ~12 and ~30 MHz, correspondingly. (b) Numerical simulation, all the parameters are the same as in (a), and $\Omega_c=1.5\Gamma$, $\Omega_p=0.35\Gamma$. FWHM of the EIT and VSOP resonances are ~12 and ~20 MHz, correspondingly.

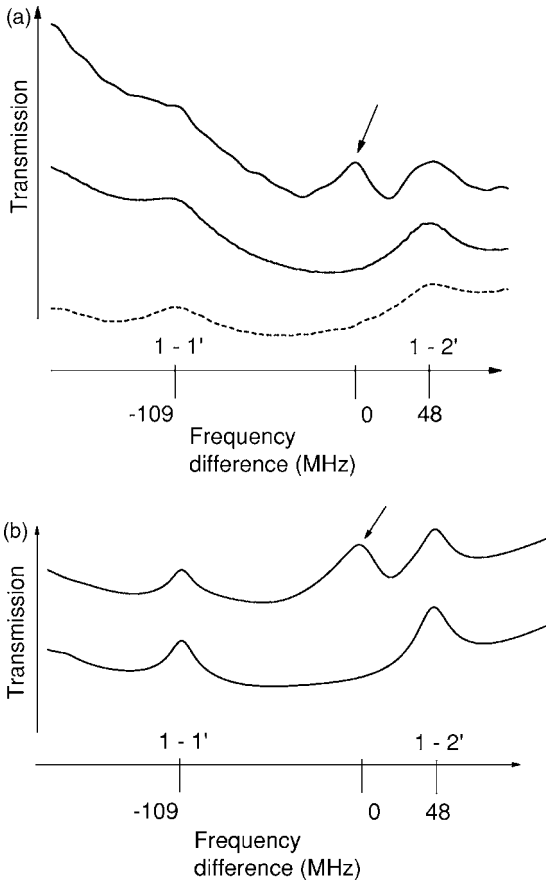

Fig. 3. Transmission spectra of the probe laser scanned across ^{87}Rb $F_g=1 \rightarrow F_e=0,1,2$ transitions when the coupling laser is red detuned by 48 MHz from the $F_g=2 \rightarrow F_e=2$ transition. The cell thickness is $L=2\lambda$ (1560 nm). (a) Experiment, $\gamma_L=5$ MHz. The middle curve is the case when the coupling laser is blocked (the curve is vertically shifted for convenience). The lower curve (dotted) presents the transmission spectra of the reference ETC1, $L=\lambda$. (b) Theoretical curve, all the parameters are the same as in (a). The Rabi frequencies of the couple and the probe lasers are $\Omega_c=2\Gamma$ and $\Omega_p=0.3\Gamma$, correspondingly. The arrow shows the EIT resonance accompanied by the VSOP resonances. The lower curve is the case when the couple is blocked.

(the accuracy of the fitting is 10% to 15%). As seen, the absorption on the $F_g=1 \rightarrow F_e=1$ transition is enhanced due to the optical "repumping" caused by the couple field, and the VSOP peak amplitude on the upper curve is smaller as compared with that on the lower curve (here the couple is blocked), indicating reduction of absorption. In Fig. 2(b), the theoretical curve is presented for the same parameters as in Fig. 2(a), with the Rabi frequencies of couple and probe lasers being $\Omega_c=1.5\Gamma$ and $\Omega_p=0.35\Gamma$, correspondingly. Here $\Gamma=6$ MHz is the lost rate of the excited states. The inset presents the results of the fitting: FWHM of the EIT and VSOP resonances are ~12 MHz and ~20 MHz, correspondingly. In both figures (a) and (b), the lower curve is vertically shifted for convenience. One can see that there is good agreement between the experiment and the theoretical model.

An interesting feature of EIT resonance formation in the ETC is the possibility of shifting the EIT resonance and VSOP peak with respect to each other on the frequency scale (this is not possible to realize in an ordinary

cell). Moreover, when the detuning is large, it is possible to completely resolve the EIT resonance (however, as shown below, this causes an additional broadening of the EIT resonance). In Fig. 3(a), the transmission spectra of the probe laser are shown for the case where the couple is red detuned by 48 MHz from the ^{87}Rb $F_g=2\rightarrow F_e=2$ transition and the probe laser is scanned across $F_g=1\rightarrow F_e=0,1,2$ transitions. The cell thickness is $L=2\lambda$ (1560 nm). The pointing arrow in the upper curve shows the EIT resonance (linewidth ~25 MHz), which is completely resolved from the accompanying VSOP resonances. The middle curve corresponds to the case where the coupling laser is blocked (the curve is vertically shifted for convenience). The lower curve (dotted) represents the transmission spectrum of the reference ETC1. In Fig. 3(b), the theoretically calculated curve is presented for the Rabi frequencies of the couple and probe lasers $\Omega_c=2\Gamma$ and $\Omega_p=0.3\Gamma$, correspondingly. The pointing arrow in the upper curve shows the EIT resonance, which is also here completely resolved from the VSOP resonances. The lower curve is the case where the coupling laser is blocked. Note that the repumping of VSOP resonances is negligible when the detuning of the coupling laser is large (see below).

As seen from Fig. 2, the coupling laser resonant with one atomic transition increases the absorption of the probe field on the other transitions due to repumping, which consequently leads to the decrease of VSOP peak amplitude. Moreover, depending on the couple field intensity, the VSOP resonances may disappear completely and with further increase of the intensity, appear reversed (increased absorption). Particularly, a sign reversal of the VSOP resonance is well seen for the transition $F_g=1\rightarrow F_e=0$ presented in Fig. 8 for the case of zero couple detuning.

In Fig. 4, the (a) experimental and (b) theoretical probe laser transmission spectra are presented for the case where the couple laser is resonant with ^{85}Rb $F_g=3\rightarrow F_e=3$ transition, with the probe laser being scanned across $F_g=2\rightarrow F_e=1,2,3$ transitions (the relevant energy levels are presented in the inset). On the upper curves of the figure [in both (a) and (b)], the VSOP resonances on $F_g=2\rightarrow F_e=1,2$ transitions (on the left from the EIT resonance pointed by the arrow) are practically absent due to repumping induced by the coupling field. The two lower curves in both (a) and (b) show the case where the coupling laser is blocked (the curves are vertically shifted for convenience). To let the reader see the contrast, the overall absorption (transmission) of the probe laser is presented in Fig. 4(c) under the same conditions as in the case of Fig. 4(a).

As mentioned above, the profiles of EIT resonances at the thicknesses $L=1.5\lambda$ and 2.5λ must be different from those at $L=\lambda$ and $L=2\lambda$. Figure 5 presents experimentally observed and calculated transmission spectra of the probe field for the cell thickness L equal to 1.5λ and 2.5λ. The pointing arrows show the EIT resonances. The two upper curves, (1) and (2), correspond to the case where the couple laser is blue detuned by 15 MHz from ^{85}Rb $F_g=3\rightarrow F_e=3$ transition and the probe laser is scanned across $F_g=2\rightarrow F_e=1,2,3$ transitions; $L=2.5\lambda$. Shown are (1) experiment (EIT resonance linewidth ~10 MHz) and

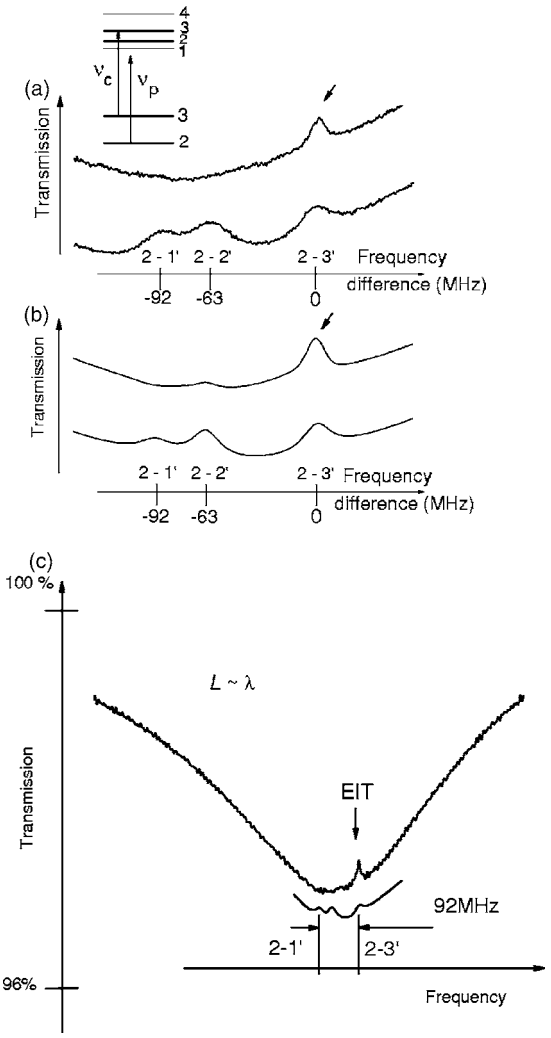

Fig. 4. Transmission spectra of the probe laser scanned across ^{85}Rb $F_g=2\rightarrow F_e=1,2,3$ transitions; the couple is resonant with $F_g=3\rightarrow F_e=3$ transition (the relevant energy levels are presented in the inset). The cell thickness $L=\lambda$ (780 nm), $\gamma_L=5$ MHz. (a) Experiment. Only the EIT resonance (pointed with the arrow on the upper curve) is present, while the VSOP resonances are absent due to a strong repumping. The lower curve presents the case when the couple is blocked (the curve is vertically shifted for convenience). (b) Numerical calculations with all the parameters are the same as in (a), $\Omega_c=1\Gamma$ and $\Omega_p=0.26\Gamma$, correspondingly. (c) Transmission spectra of the probe laser under the same conditions as in (a).

(2) calculated spectra with $\Omega_c=1\Gamma$, $\Omega_p=0.2\Gamma$, $\gamma_L=5$ MHz. Curves (3) and (4) correspond to the case where the coupling laser is resonant with ^{85}Rb $F_g=3\rightarrow F_e=3$ transition; $L=1.5\lambda$: (3) experiment and (4) calculated spectra with $\Omega_c=1\Gamma$, $\Omega_p=0.1\Gamma$, $\gamma_L=5$ MHz. Curve (5) is the transmission spectrum of the reference ETC1, $L=\lambda$. As can be seen, there are no VSOP resonances of reduced absorption in Fig. 5 that are present in Figs. 2 and 3. Note that in the case of $L=\lambda$ and 2λ, the EIT peak (when the coupling laser is in resonance with the atomic transition) is superimposed on the VSOP peak, which is also a peak of reduced absorption. However, in the case of $L=1.5\lambda$ and $L=2.5\lambda$, the EIT peak is superimposed on the VSOP peak, which is now the peak of increased absorption (due to the coherent Dicke effect [12–15]). That is why, in the second case, the

EIT peak demonstrates a small increase in the absorption on the wings, and further, a decrease of the absorption [see curves (3) and (4) in Fig. 5]. Another distinction in the behavior of the VSOP resonances accompanying the EIT resonance is seen when comparing the "sign" of the VSOP resonances in Figs. 2, 3, and 5.

Figure 6 shows the calculated EIT resonance linewidth as a function of the laser radiation spectral width. The dependence is obtained by fitting the theoretical probe transmission curves when the couple is resonant with $F_g=2\rightarrow F_e=2$ transition (for other parameters see the figure caption). It is seen that the EIT width increases linearly with the laser spectral linewidth. From the figure it is seen that even in the case of zero laser linewidths, the residual linewidth of the EIT is 9 MHz. This linewidth is composed of Γ_{21} and the additional broadening due to coupling and probe laser intensities.

Figure 7 presents the calculated transmission spectrum of the probe field at the cell thickness $L=\lambda/2$ (390 nm) for the case where the coupling laser is resonant with ^{85}Rb $F_g=3\rightarrow F_e=3$ transition (for other parameters see the figure caption). Dotted curve (1) corresponds to the case where the coupling laser is blocked. Note, that in both cases, (1) and (2), there is an increased absorption on VSOP resonances, opposite from the case of $L=\lambda$ and 2λ. The pointing arrow on curve (2) shows the EIT resonance peak. Hence, it is possible to observe EIT resonance at the cell thickness $L=\lambda/2$ choosing correct experimental parameters and using coherently coupled lasers [2–4] with a small spectral linewidth of radiation. This is a remarkable result since previous experimental studies have shown that using only the probe laser, even at high radiation intensity ~ 1 W/cm^2 it is not possible to obtain a VSOP resonance at the cell thickness $L=\lambda/2$ [12,15]. Impossibility to obtain a VSOP resonance of reduced absorption at $L=\lambda/2$ was also confirmed by theoretical considerations (in contrast, ~ 1 mW/cm^2 is sufficient to form VSOP dips at $L=\lambda$ [14]). This is because of a strong Dicke-type coherent narrowing regime at $L=\lambda/2$, meanwhile as we can see from Fig. 7, the EIT effect allows one to form a narrow dip of reduced absorption for $L=\lambda/2$ at a lower laser intensity. Moreover, the theoretical model presented shows that, under certain conditions, it is possible to form the EIT resonance for $L<100$ nm as well. In [22] atom-surface van der Waals interaction when $L<100$ nm is successfully studied exploits transmission and selective reflection spectra. The implementation of the EIT effect could give an additional possibility for studying atom-surface interaction via the frequency shift of the EIT resonance.

In Fig. 8, the calculated probe field transmission spectra are shown for different values of the blue detuning of the couple field with respect to the ^{87}Rb, $F_g=2\rightarrow F_e=2$ transition frequency for $L=\lambda$ (for other parameters see the figure caption). We have chosen the blue detuning in order to see a pure dependence from the detuning, meanwhile in the case of red detuning, the transition $F_g=1\rightarrow F_e=1$ will have an influence on the EIT resonance. As can be seen, the narrowest EIT resonance is observed

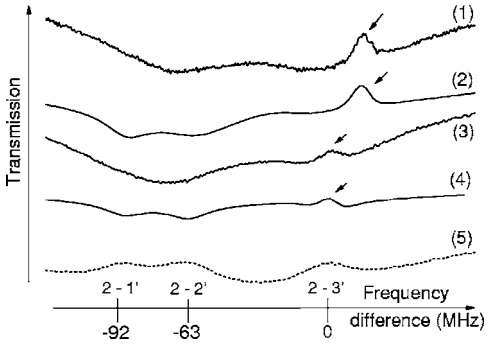

Fig. 5. Transmission spectra of the probe laser scanned across ^{85}Rb $F_g=2\rightarrow F_e=1,2,3$ transitions. (1) and (2) refer to the coupling laser blue detuned by 15 MHz from $F_g=3\rightarrow F_e=3$ transition; the cell thickness is $L=2.5\lambda$. The pointing arrows show the EIT resonances: (1) experiment and (2) numerical calculations. (3) and (4) refer to the case where the couple is resonant with $F_g=3\rightarrow F_e=3$ transition, the cell thickness $L=1.5\lambda$: (3) experiment and (4) numerical calculations. (5) The transmission spectrum of the reference ETC1, $L=\lambda$.

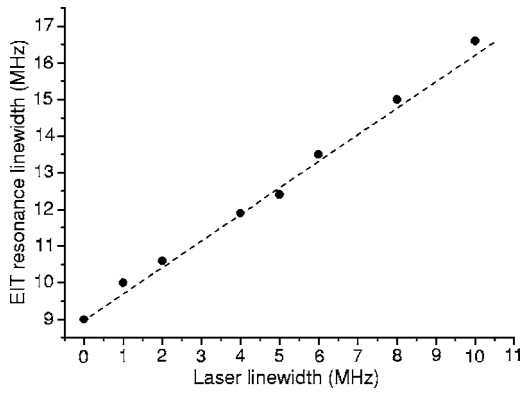

Fig. 6. Calculated linewidth of the EIT resonance as a function of the laser radiation spectral width (couple and probe are assumed to have the same linewidth). The coupling laser is resonant with ^{87}Rb $F_g=2\rightarrow F_e=2$ transition, cell thickness $L=\lambda$ (780 nm), $\Omega_c=1.5\Gamma$, $\Omega_p=0.35\Gamma$.

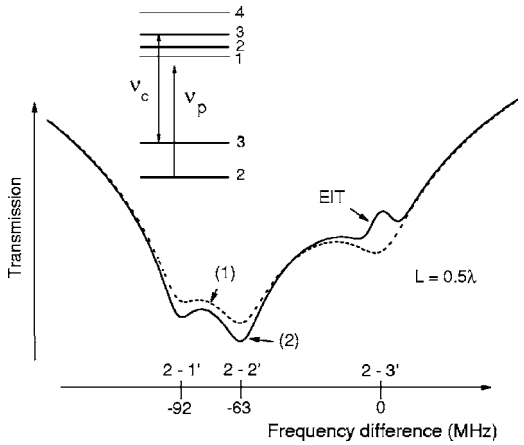

Fig. 7. Calculated transmission spectra of the probe field for the cell thickness $L=\lambda/2$ (390 nm) when the couple is resonant ^{85}Rb $F_g=3\rightarrow F_e=3$ transition (the relevant energy levels are presented in the inset); $\gamma_L=1$ MHz, $\Omega_c=1\Gamma$, $\Omega_p=0.3\Gamma$. (1) the couple beam is blocked, (2) the couple is on. EIT resonance on curve (2) is marked by an arrow. A possibility to observe EIT resonance at the cell thickness $L=\lambda/2$ is a remarkable result (see the text). Also on curve (2), the increase of absorption on VSOP resonances on $F_g=2\rightarrow F_e=1,2$ transitions is observable [compare with curve (1)].

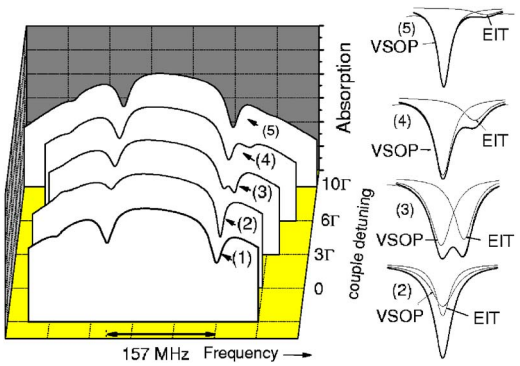

Fig. 8. (Color online) Calculated probe field transmission spectra as a function of the blue detuning of the couple field frequency from the ^{87}Rb, $F_g=2\rightarrow F_e=2$ transition. The cell thickness $L=\lambda$ (780 nm), $\gamma_L=1$ MHz, $\Omega_c=1.5\Gamma$, $\Omega_p=0.35\Gamma$, $\Gamma=6$ MHz. (1) dashed curve, coupling laser is blocked, (2) coupling laser is resonant with $F_g=2\rightarrow F_e=2$ transition, (3) couple laser is blue detuned by 3Γ, (4) by 6Γ, (5) by 10Γ. $\gamma_{EIT}=12$, 16, 25, and 36 MHz for (2), (3), (4), and (5), correspondingly; $\gamma_{VSOP}\sim 18$ MHz for all cases (2)–(5).

when the coupling laser is resonant with the $F_g=2\rightarrow F_e=2$ transition, whereas the increase of the coupling field detuning leads to a rapid broadening of the EIT resonance. With the increase of the blue detuning from 0Γ to 10Γ, the width of EIT resonance γ_{EIT} increases from 12 to 36 MHz. It is important to note that in cells of usual length (1–10 cm), the width and amplitude of EIT resonance have a weak dependence on coupling field detuning (for a physical explanation, see below). It is also interesting to note that the widths of VSOP resonances remain practically unchanged with the increase of the coupling field detuning (for the four cases presented in the figure, the width of VSOP resonance γ_{VSOP} is equal to ~18 MHz). This is clearly seen for the VSOP peak on the $F_g=1\rightarrow F_e=1$ transition.

To provide comparison of the EIT process and VSOP formation with the cell of an ordinary length (COL), in Fig. 9, the transmission spectrum of the probe laser (upper curve) is shown when the coupling laser (~0.5 mW) is resonant with the ^{85}Rb $F_g=3\rightarrow F_e=2$ transition, while the probe laser (~0.3 mW) is scanned across $F_g=2\rightarrow F_e=1,2,3$ transitions (both beams are parallel, and the COL is inserted inside Helmholtz coils). The cell length is ~1 cm, and the temperature is ~40°C. In the upper curve, the EIT resonance (mentioned by the pointing arrow) is seen together with seven sub-Doppler VSOP resonances. The EIT resonance has the linewidth of 2–3 MHz (i.e., approximately two times less than the natural linewidth). The lower curve is the transmission spectrum of the ETC1 for $L=\lambda$ (this spectrum serves as a reference for the calibration of the frequency scale).

The following significant distinctions for EIT and VSOP formations are observed when using the ETC with an atomic vapor column of $L\sim\lambda$ as compared with the COL:

1. In the case of exact collinear propagation of the two laser beams in the COL, the number of sub-Doppler satellites is equal to 7 (see Fig. 9), while under the well-defined geometry of the interaction the number of VSOP peaks can be reduced to 5 [23]. Note that the EIT resonance is always superimposed on one of the VSOP resonances (the VSOP number 2 in Fig. 9). When using ETC, the maximal number of VSOP resonances is equal to 3; the corresponding resonance frequencies are fixed and do not depend on the coupling laser frequency [9]. The EIT resonance can be superimposed on one of these VSOP resonances depending on the coupling laser frequency only if the coupling laser frequency is in exact resonance with the corresponding atomic transition. However, when the coupling laser is detuned from the resonance with the transition, the EIT peak can be clearly resolved on the frequency scale (see Fig. 3).

2. In the case of the COL, the frequency position of the VSOP resonance is determined by the coupling laser frequency and by the values of the hyperfine splittings of the ground and excited states. Note that the frequencies of VSOP resonances become larger with the increase of coupling laser frequency and smaller when this frequency is reduced [24]. In contrast, in the case of the ETC, all three VSOP resonances are positioned on the atomic transitions. This is explained by the fact that the optical pumping is more effective for the atoms with small longitudinal velocity, and that the main contribution to the resonant signal comes from the atoms flying parallel to the cell windows, perpendicularly to the laser beam and, consequently, having negligible Doppler shift. Thus, independently of the ratio of the coupling and probe laser intensities, the positions of the VSOP resonances on the frequency scale (in the case of the COL) and EIT resonance (for both the COL and the ETC) depend only on the frequency of the coupling laser.

3. In the case of the COL, when the coupling laser is detuned from the exact resonance by a value Δ, only the atoms with certain longitudinal velocity will participate in the formation of the EIT resonance. For the particular case of ^{87}Rb when the coupling laser is tuned from $F_g=2$, with the probe field being scanned across the set of hyperfine transitions $F_g=1\rightarrow F_e=0,1,2$ this velocity is equal to

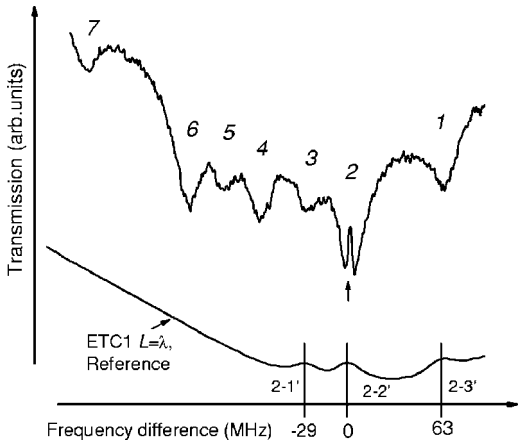

Fig. 9. Transmission spectrum of the probe laser (upper curve), when the coupling laser is resonant with the ^{85}Rb $F_g=3\rightarrow F_e=2$ transition, while the probe laser is scanned across $F_g=2\rightarrow F_e=1,2,3$ transitions. The cell length is ~1 cm, and the temperature is ~40°C. In the upper curve, the EIT resonance (with the linewidth of 2–3 MHz and mentioned by the pointing arrow) is seen together with seven VSOP resonances. The lower curve is the transmission spectrum of the ETC1 for the $L=\lambda$ and serves as a reference for the calibration of the frequency scale.

$v_{1,2}=2\pi(\nu_c-\nu_{2i})/k$, where $i=1,2$ with k being the wavenumber of the irradiating field. For simplicity, we consider that the wavenumbers are the same for the probe and coupling lasers. Since the atoms obey the Maxwellian distribution, the number of atoms with the corresponding velocity projections $v_{1,2}$ decreases with the increase of the couple laser detuning Δ, thus resulting in weakening of the EIT resonance. Note, that if $v_{1,2}<v_T$, where v_T is the most probable thermal velocity, the weakening of the EIT resonance is rather slow. As for the EIT width, it practically does not change (moreover, as shown in [25], the formation of EIT resonance on the wings of the Doppler profile of the absorption line can lead to its narrowing).

For the opposite, in the case of the ETC, the most narrow and the most contrasting EIT resonance is formed when the coupling laser is resonant with the corresponding atomic transition, meanwhile the increase of the coupling laser detuning leads to the broadening and worsening of the contrast of the EIT resonance (see Fig. 8). The physical explanation of this fact is that when the couple laser is detuned from the corresponding transition by a value of Δ, only the atoms having the velocity projections $v_{1,2}=2\pi\Delta/k$ participate in the formation of EIT, and for these atoms the time of flight between the cell windows is less than that when $v_z=0$. This leads to the increase of Γ_{21} and, consequently, to the broadening and contrast reduction of the EIT resonance.

4. In a COL, the EIT resonance width and contrast are weakly influenced by the cell length, while in the case of ETC, the EIT resonance line shape depends on whether the cell length is equal to $L=n\lambda$ or to $L=(2n+1)\lambda/2$. As for the VSOP resonances, in a COL, they demonstrate the increasing of the absorption (see Fig. 9) and are weakly influenced by the cell length, while in the case of ETC, their sign is different for $L=n\lambda$ and for $L=(2n+1)\lambda/2$ (Figs. 2 and 3; compare with Fig. 5).

5. Note that in the ETC, there is a difference in the behavior of the VSOP and EIT resonances in the case when the coupling laser is detuned from the atomic transitions. In particular, from Figs. 3 and 8, it can be seen that the "repumping" caused by the detuning from the transition center coupling laser is almost vanishing, while at similar conditions, the EIT resonance is still well pronounced. On the contrary, for the case of the COL (see Fig. 9), the EIT resonance is superimposed on VSOP resonance (number 2) of increased absorption (due to the repumping effect) at any coupling frequency.

In [9], it was shown that by using the ETC, one can measure the magnitude of the magnetic field by the splitting of EIT resonances. Use of the COL yields much higher B-field sensitivity [4] due to narrower EIT resonances. Nevertheless, the ETC provides micrometer-spatial resolution and is advantageous for the measurement of highly nonhomogeneous magnetic fields. The latter is important for atomic magneto-optical cooling, nuclear magnetic resonance spectroscopy, and magnetic resonance tomography, synchrotron radiation sources, heavy mineral separation, and other applications.

5. CONCLUSIONS

We have studied the peculiarities of the EIT effect with the help of the ETC with the thickness of the Rb vapor column of the order of light wavelength λ (780 nm), varying in the range of $0.5\lambda-2.5\lambda$. Λ-systems on the D_2 line of ^{85}Rb and ^{87}Rb have been studied experimentally. Along with EIT resonance, we have studied the VSOP resonance, which are the satellites of EIT resonance. As a rule, the VSOP resonances are spectrally broader than the EIT resonances. A number of dramatic differences of the EIT and VSOP resonance formation in the ETC in comparison with ordinary (centimeter-size) cells is revealed. Particularly, in the case of the ETC, the EIT linewidth and contrast dramatically depend on the coupling laser detuning from the exact atomic transition. The developed theoretical model takes into account the peculiarities of the transmission spectra when $L=n\lambda$ and $L=(2n+1)\lambda/2$ and describes the experiment well. The dependence of EIT resonance on the probe and coupling laser intensities, couple detuning from atomic resonance, and laser spectral linewidth are also studied. The possibility of the EIT resonance formation when the vapor column thickness is $L=0.5\lambda$ or even less is theoretically predicted. Presented peculiarities of the EIT effect when the thickness of the atomic column vapor $L\sim\lambda$ (in our case $L=780$ nmfor the Rb D_2 line) are of a general nature, and this means that similar results are expected for Li, Na, K, and Cs atomic vapors, but for the other values, the thickness corresponding to the resonant wavelength, for example, for the Na D_2 line, is $L\sim590$ nm.

APPENDIX A

The density-matrix equations of motion for the system shown in Fig. 1 in the rotating frame are explicitly written as

$$\dot{\rho}_{11}=-2\,\mathrm{Im}(\Omega_1^*\rho_{31})-2\,\mathrm{Im}(\Omega_2^*\rho_{41})-2\,\mathrm{Im}(\Omega_3^*\rho_{51})+\gamma_{31}\rho_{33}+\gamma_{41}\rho_{44}+\gamma_{51}\rho_{55},$$

$$\dot{\rho}_{22}=-2\,\mathrm{Im}(\Omega_4^*\rho_{42})-2\,\mathrm{Im}(\Omega_5^*\rho_{52})-2\,\mathrm{Im}(\Omega_6^*\rho_{62})+\gamma_{42}\rho_{44}+\gamma_{52}\rho_{55}+\gamma_{62}\rho_{66},$$

$$\dot{\rho}_{33}=2\,\mathrm{Im}(\Omega_1^*\rho_{31})-\Gamma_{33}\rho_{33},$$

$$\dot{\rho}_{44}=2\,\mathrm{Im}(\Omega_2^*\rho_{41})+2\,\mathrm{Im}(\Omega_4^*\rho_{42})-\Gamma_{44}\rho_{44},$$

$$\dot{\rho}_{55}=2\,\mathrm{Im}(\Omega_3^*\rho_{51})+2\,\mathrm{Im}(\Omega_5^*\rho_{52})-\Gamma_{55}\rho_{55},$$

$$\dot{\rho}_{66}=2\,\mathrm{Im}(\Omega_6^*\rho_{62})-\Gamma_{66}\rho_{66},$$

$$\dot{\rho}_{62}=i\Omega_6(\rho_{22}-\rho_{66})-i\Omega_4\rho_{64}-i\Omega_5\rho_{65}-(i\Delta_6^c+\Gamma_{62})\rho_{62},$$

$$\dot{\rho}_{52}=i\Omega_5(\rho_{22}-\rho_{55})+i\Omega_3\rho_{12}-i\Omega_4\rho_{54}-i\Omega_6\rho_{56}-(i\Delta_5^c+\Gamma_{52})\rho_{52},$$

$$\dot{\rho}_{42}=i\Omega_4(\rho_{22}-\rho_{44})+i\Omega_2\rho_{12}-i\Omega_5\rho_{45}-i\Omega_6\rho_{46}-(i\Delta_4^c+\Gamma_{42})\rho_{42},$$

$$\dot{\rho}_{32} = i\Omega_1\rho_{12} - i\Omega_4\rho_{34} - i\Omega_5\rho_{35} - i\Omega_6\rho_{36} - [i(\Delta_5^c - \delta_1 - \delta_2) + \Gamma_{32}]\rho_{32},$$

$$\dot{\rho}_{61} = i\Omega_6\rho_{21} - i\Omega_2\rho_{64} - i\Omega_3\rho_{65} - i\Omega_1\rho_{63} - [i(\Delta_6^c + \Delta_R) + \Gamma_{61}]\rho_{61},$$

$$\dot{\rho}_{51} = i\Omega_3(\rho_{11} - \rho_{55}) + i\Omega_5\rho_{21} - i\Omega_1\rho_{53} - i\Omega_2\rho_{54} - [i\Delta_3^p + \Gamma_{51}]\rho_{51},$$

$$\dot{\rho}_{41} = i\Omega_2(\rho_{11} - \rho_{44}) + i\Omega_4\rho_{21} - i\Omega_1\rho_{43} - i\Omega_3\rho_{45} - [i\Delta_2^p + \Gamma_{41}]\rho_{41},$$

$$\dot{\rho}_{31} = i\Omega_1(\rho_{11} - \rho_{33}) - i\Omega_2\rho_{34} - i\Omega_3\rho_{35} - [i\Delta_1^p + \Gamma_{31}]\rho_{31},$$

$$\dot{\rho}_{65} = -i\Omega_3^*\rho_{61} + i\Omega_6\rho_{25} - i\Omega_5^*\rho_{62} - [i\delta_3 + \Gamma_{65}]\rho_{65},$$

$$\dot{\rho}_{64} = -i\Omega_2^*\rho_{61} + i\Omega_6\rho_{24} - i\Omega_4^*\rho_{62} - [i(\delta_2 + \delta_3) + \Gamma_{64}]\rho_{64},$$

$$\dot{\rho}_{63} = -i\Omega_1^*\rho_{61} + i\Omega_6\rho_{23} - [i(\delta_1 + \delta_2 + \delta_3) + \Gamma_{63}]\rho_{63},$$

$$\dot{\rho}_{54} = i\Omega_3\rho_{14} + i\Omega_2^*\rho_{51} + i\Omega_5\rho_{24} - i\Omega_4^*\rho_{52} - [i\delta_2 + \Gamma_{54}]\rho_{54},$$

$$\dot{\rho}_{53} = i\Omega_3\rho_{13} - i\Omega_1^*\rho_{51} + i\Omega_5\rho_{23} - [i(\delta_1 + \delta_2) + \Gamma_{53}]\rho_{53},$$

$$\dot{\rho}_{43} = i\Omega_2\rho_{31}^* - i\Omega_1^*\rho_{41} + [i\delta_1 + \Gamma_{43}]\rho_{43},$$

$$\dot{\rho}_{21} = -i\Omega_1\rho_{32}^* + i\Omega_4^*\rho_{41} - i\Omega_2\rho_{42}^* + i\Omega_5^*\rho_{51} - i\Omega_3\rho_{52}^* + i\Omega_6^*\rho_{61} - [i\Delta_R + \Gamma_{21}]\rho_{21},$$

and $\rho_{ij} = \rho_{ji}^*$. Here γ_{i1} $(i = 3,4,5)$ are the population relaxation rates from state $|i\rangle$ to state $|1\rangle$, and γ_{j2} $(j = 4,5,6)$ are the population relaxation rates from state $|j\rangle$ to state $|2\rangle$;

$$\Gamma_{ii} = \sum_{i \neq j} \gamma_{ij} \quad (i = 3,4,5,6;\ j = 1,2)$$

are the total decay rates out of state $|i\rangle$. Off-diagonal coefficients

$$\Gamma_{ij} = \frac{1}{2}\left(\sum_k \gamma_{ik} + \sum_l \gamma_{jl}\right)$$

are decoherence decay rates, where k denotes all the levels into which the population from level i may decay and l denotes all the levels into which the population from level j may decay; $\Omega_1 = \mu_{13}E_p/2\hbar$, $\Omega_2 = \mu_{14}E_p/2\hbar$, $\Omega_3 = \mu_{15}E_p/2\hbar$ are the Rabi frequencies of the probe field; $\Omega_4 = \mu_{24}E_c/2\hbar$, $\Omega_5 = \mu_{25}E_c/2\hbar$, $\Omega_6 = \mu_{26}E_c/2\hbar$ are the Rabi frequencies of the couple field. δ_1, δ_2, δ_3 are the hyperfine splittings of the upper levels, and Δ_R is the two-photon Raman detuning.

ACKNOWLEDGMENTS

The authors thank A. Sarkisyan for his valuable participation in the fabrication of the ETC as well as to Yu. Malakyan for discussions and A. Nersisyan for the curves fitting. This work was supported, in part, by the Armenian National Science and Education Fund (ANSEF) grant 05-PS-opt-0813-233 and Scientific Co-operation between Eastern Europe and Switzerland (SCOPES) grant IB7320-110684/1 and the International Association for Cooperation with Scientists from the former Soviet Union (INTAS) South-Caucasus grant 06-1000017-9001.

REFERENCES

1. G. Alzetta, A. Gozzini, L. Moi, and G. Orriols, "An experimental method for the observation of the RF transition and laser beat resonance in oriented Na vapour," in Nuovo Cimento Soc. Ital. Fis., B **36**, 5–20 (1976).
2. E. Arimondo, "Coherent population trapping in laser spectroscopy," in *Progress in Optics*, Vol. 35, E. Wolf, ed. (Elsevier, 1996) pp. 257–354.
3. S. Harris, "Electromagnetically induced transparency," Phys. Today **50**, 36–42 (1997).
4. R. Wynands and A. Nagel, "Precision spectroscopy with coherent dark states," Appl. Phys. B **68**, 1–25 (1999) and references therein.
5. E. B. Alexandrov, "Recent progress in optically pumped magnetometers," Phys. Scr., T **105**, 27–30 (2003).
6. S. Knappe, L. Hollberg, and J. Kitching, "Dark-line atomic resonances in submillimeter structures," Opt. Lett. **29**, 388–390 (2004).
7. D. Budker, V. Yashchuk, and M. Zolotorev, "Nonlinear magneto-optic effects with ultra narrow widths," Phys. Rev. Lett. **81**, 5788–5791 (1998).
8. D. Petrosyan and Yu. Malakyan, "Electromagnetically induced transparency in a thin vapor film," Phys. Rev. A **61**, 053820 (2000).
9. A. Sargsyan, D. Sarkisyan, and A. Papoyan, "Dark-line atomic resonances in a submicron-thin Rb vapor layer," Phys. Rev. A **73**, 033803 (2006).
10. D. Sarkisyan, D. Bloch, A. Papoyan, and M. Ducloy, "Sub-Doppler spectroscopy by submicron thin Cs-vapor layer," Opt. Commun. **200**, 201–208 (2001).
11. E. A. Gazazyan, A. V. Papoyan, D. Sarkisyan, and A. Weis, "Laser frequency stabilization using selective reflection from a vapor cell with a half-wavelength thickness," submitted to Laser Phys. Lett.
12. G. Dutier, A. Yarovitski, S. Saltiel, A. Papoyan, D. Sarkisyan, D. Bloch, and M. Ducloy, "Collapse and revival of a Dicke-type coherent narrowing in a sub-micron thick vapor cell transmission spectroscopy," Europhys. Lett. **63**, 35–41 (2003).
13. G. Dutier, S. Saltiel, D. Bloch, and M. Ducloy, "Revising optical spectroscopy in a thin vapor cell: mixing of reflection and transmission as a Fabry–Perot microcavity effect," J. Opt. Soc. Am. B **20**, 793–800 (2003).
14. D. Sarkisyan, T. Varzhapetyan, A. Sarkisyan, Yu. Malakyan, A. Papoyan, A. Lezama, D. Bloch, and M. Ducloy, "Spectroscopy in an extremely thin vapor cell: comparing the cell-length dependence in fluorescence and in absorption techniques," Phys. Rev. A **69**, 065802 (2004).
15. D. Sarkisyan, T. Varzhapetyan, A. Papoyan, D. Bloch, and M. Ducloy, "Absorption and fluorescence in atomic submicron cell: high laser intensity case," in *ICONO 2005: Nonlinear Laser Spectroscopy, High Precision Measurements, and Laser Biomedicine and Chemistry*, S. N. Bagayev, A. Chikishev, A. Dmitriev, M. Ducloy, Y. Heinz, V. Letokhov, A. Shkurinov, and H. Takahashi, eds., Proc. SPIE **6257**, 625701 (2006).
16. J. H. Eberly, "Atomic relaxation in the presence of intense partially coherent radiation fields," Phys. Rev. Lett. **37**, 1387–1390 (1976).
17. G. S. Agarwal, "Exact solution for the influence of laser temporal fluctuations on resonance fluorescence," Phys. Rev. Lett. **37**, 1383–1386 (1976).

18. P. Zoller, "Fokker–Planck equation treatment of atomic relaxation and resonance fluorescence in phase-modulated laser light," J. Phys. B **10**, L321–L324 (1977).
19. G. S. Agarwal, "Quantum statistical theory of optical-resonance phenomena in fluctuating laser fields," Phys. Rev. A **18**, 1490–1506 (1978).
20. B. J. Dalton and P. L. Knight, "Population trapping and ultranarrow Raman lineshapes induced by phase-fluctuating fields," Opt. Commun. **42**, 411–416 (1982).
21. G. Nikogosyan, D. Sarkisyan, and Yu. Malakyan, "Absorption of resonance radiation and fluorescence of a layer of an atomic gas with thickness of the order of a wavelength," J. Opt. Technol. **71**, 602–607 (2004).
22. I. Hamdi, P. Todorov, A. Yarovitski, G. Dutier, I. Maurin, S. Saltiel, Y. Li, A. Lezama, T. Varzhapetyan, D. Sarkisyan, M.-P. Gorza, M. Fichet, D. Bloch, and M. Ducloy, "Laser spectroscopy with nanometric gas cells: distance dependence of atom-surface interaction and collisions under confinement," Laser Phys. **15**, 987–996 (2005).
23. A. Sargsyan, D. Sarkisyan, D. Staedter, and A. M. Akulshin, "Doppler-free satellites of resonances of electromagnetically induced transparency and absorption on the D_2 lines of alkali metals," Opt. Spectrosc. **101**, 762–768 (2006).
24. Z. D. Liu, P. Juncar, D. Bloch, and M. Ducloy, "Raman polarization-selective feedback schemes for all-optical microwave frequency standards," Appl. Phys. Lett. **69**, 2318–2320 (1996).
25. J. Wang, Y. Wang, S. Yan, T. Liu, and T. Zhang, "Observation of sub-Doppler absorption in the Λ-type three-level Doppler-broadened cesium system," Appl. Phys. B: Lasers Opt. **78**, 217–220 (2004).